INTERNATIONAL ATOMIC ENERGY AGENCY
UNITED NATIONS EDUCATIONAL, SCIENTIFIC AND CULTURAL ORGANIZATION
INTERNATIONAL CENTRE FOR THEORETICAL PHYSICS
I.C.T.P., P.O. BOX 586, 34100 TRIESTE, ITALY, CABLE: CENTRATOM TRIESTE

H4.SMR/449-40

WINTER COLLEGE ON
HIGH RESOLUTION SPECTROSCOPY

(8 January - 2 February 1990)

LASER WITH FEEDBACK: AN OPTICAL IMPLEMENTATION OF COMPETING INSTABILITIES, SHIL'NIKOV CHAOS, AND TRANSIENT FLUCTUATION ENHANCEMENT

T. Arecchi & R. Meucci

Istituto Nazionale di Ottica
Firenze 50125 Arcetri
Italy

Laser with feedback: an optical implementation of competing instabilities, Shil'nikov chaos, and transient fluctuation enhancement

F. T. Arecchi, W. Gadomski,
A. Lapucci, H. Mancini,
R. Meucci, and J. A. Roversi

a reprint from Journal of the Optical Society of America B
volume 5, number 5, May 1988

Laser with feedback: an optical implementation of competing instabilities, Shil'nikov chaos, and transient fluctuation enhancement

F. T. Arecchi, W. Gadomski,* A. Lapucci, H. Mancini,† R. Meucci, and J. A. Roversi‡

Istituto Nazionale di Ottica, 50125 Firenze, Italy

Received October 26, 1987; accepted January 4, 1988

A CO_2 laser with feedback shows different dynamic regimes depending on the dominant role of one or two of three coexisting unstable stationary points. These regimes have been characterized by statistical distributions of return times to a Poincaré section at constant intensity. In particular, in the regime of Shil'nikov chaos the iteration maps of return times display a statistical spread owing to a transient fluctuation enhancement phenomenon peculiar to macroscopic systems, which is absent in low-dimensional chaotic dynamics.

INTRODUCTION

The dynamic behavior of a single-mode CO_2 laser with feedback is characterized by global features in the phase space, related to the presence of three coexisting unstable fixed points. As a control parameter is monotonically increased, one can observe transitions from a Hopf bifurcation to a local chaos and eventually to regular spiking and Shil'nikov chaos. Furthermore, one can find evidence of competition among these different kinds of instability.[1] The phase-space trajectories are affected differently by each of the three unstable points, and by adjustment of the control parameters they can be characterized by the dominant role of only one, or a pair, of them.

A linear stability analysis shows the local features at each fixed point. To be precise, point 0 (at zero intensity) is a saddle node with two stable directions and one unstable; point 1 has a plane unstable manifold with a focus and a stable third direction; point 2 has a stable manifold with a focus and an unstable third direction. Shil'nikov chaos is related to the saddle focus character of point 2.[2] Around a saddle focus the motion consists of a contracting spiral $\exp(-\lambda t)\cos(\omega t)$ on the stable manifold and of an exponential expansion $\exp(\gamma t)$ along the unstable manifold. The presence of the other two unstable points ensures that the diverging flow is reinjected into the neighborhood of the saddle focus. Shil'nikov showed that for $|\lambda| < \gamma$ there exists a countable set of unstable trajectories close to the homoclinic one.[2] This structure of the flow is one of the simplest capable of generating chaotic behavior in many autonomous systems, such as the Lorenz equations[3] and the Belousov–Zhabotinski reaction.[4]

The temporal behavior of laser output intensity in this regime is characterized by pulses almost equal in shape but with chaotic recurrence times.[5] The regularity in shape means that the points at any Poincaré section are so closely packed that impossibly precise measurements of their position would be required if the relevant features of the motion were to be found. Instead, there is a large spread in the return times to a Poincaré section close to the unstable point. For this reason, the statistics of the return times appears to be the most appropriate characterization of Shil'nikov chaos.[5]

Our experimental data yield iteration maps of return times in close agreement with those arising from the theory of Shil'nikov. However, the theory must be supplemented by the consideration of experimental iteration maps of finite thickening independent of the accuracy of measurement. This is due to a transient fluctuation enhancement discovered earlier in the decay of an unstable state of a macroscopic system.[6–8] Even though this spread has no relevance to the average dynamics, it contributes a large transient fluctuation whenever the system decays from an unstable point.

A heuristic explanation of these fluctuations (the transient counterpart of the stationary critical fluctuations at a phase transition) is as the follows.[6–8] For a dynamic system made of N degrees of freedom the relative fluctuations at a stationary point are $O(1/N)$. If the point is unstable, the linear part of the decay implies an amplification that scales as the system size, $O(N)$. Hence the amplified relative fluctuations will be $O(1)$ and the corresponding absolute fluctuations scale as the system size. Here we observe this enhancement repeated at each Poincaré cycle. Large fluctuations of this type were first observed in the switch-on of a laser[6] and then in many quenching phenomena, such as spinodal decomposition and superfluorescence.[7] Our finding allows us to draw a line of demarcation between chaotic experiments on large systems and simulations on simplified low-dimensional models.

EXPERIMENTAL SETUP

Our experimental setup (Fig. 1) consists of a single-mode CO_2 laser with an intracavity electro-optic modulator yielding cavity losses proportional to the laser output intensity.[9] The optical cavity is defined by a grating in order to select the $P(20)$ line at 10.6 μm and a total reflecting mirror mounted an a piezoelectric translator to adjust the frequency of the cavity mode to the center of the molecular line. The cavity

0740-3224/88/051153-07$02.00

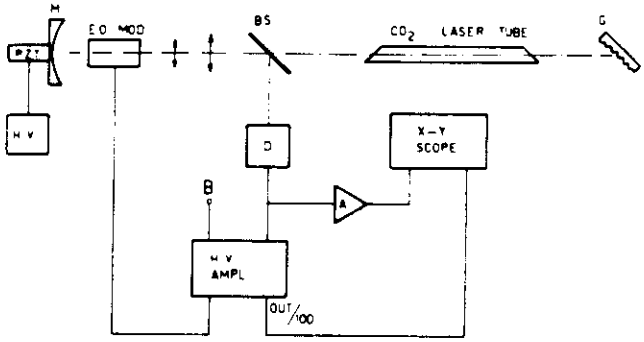

Fig. 1. Experimental setup. M, total reflecting mirror mounted on a piezoelectric (P.Z.T.) drive; E.O. MOD, electro-optic modulator; B.S., ZnSe beam splitter; G, grating; D, HgCdTe detector; B, bias voltage; H.V., high-voltage amplifier; A, amplifier.

length is 2 m. The radiation is coupled out by means of a low-reflectivity ZnSe beam splitter and detected by a HgCdTe detector. The output signal, suitably amplified and added to a continous voltage, is sent to the electro-optic modulator, which has a voltage $V_{\lambda/2} = 4240$ V.

For a fixed pump parameter proportional to the discharge current in the laser tube, our system has two control parameters: the bias voltage applied to the electro-optic modulator and the gain in the feedback loop.

THEORETICAL MODEL

The CO_2 laser represents one of the most appropriate systems to use in investigating low-dimensional chaotic dynamics. Its dynamic behavior can be described by two coupled differential equations, one for the field amplitude and the other for the population inversion, the fast polarization being adiabatically eliminated from the complete set of Maxwell–Bloch equations.[10]

The third degree of freedom crucial for the onset of deterministic chaos can be provided in one of several ways: (i) by an external sinusoidal drive applied to an intracavity electro-optic modulator that controls the cavity losses[11] or the cavity length,[12] (ii) by injection of a field from an external detuned laser,[13] (iii) by a ring configuration, which decouples forward and backward waves, thus contributing at least one extra degree of freedom.[14]

In our configuration the presence of feedback introduces the third degree of freedom. When the feedback loop is so fast that it provides a practically instantaneously adapted loss coefficient, it does not modify the phase-space topology, which in the case of a CO_2 laser remains two dimensional. On other hand, if the time scale of the feedback loop is of the same order as of the other two relevant variables, the system becomes three dimensional. Such a system is described by three first-order differential equations for the laser intensity $x(t)$, the population inversion $y(t)$, and the modulation voltage $z(t)$ as follows:

$$\dot{x} = -K_0 x[1 + \alpha \sin^2(z) - y], \tag{1}$$

$$\dot{y} = -\gamma_{\parallel}(y + xy - A), \tag{2}$$

$$\dot{z} = -\beta(z - B + rx), \tag{3}$$

where $K_0 = (c/L)T$ is the unmodulated cavity-loss parameter, L is the cavity length, T is the effective transmission of the cavity, and $\gamma_{\parallel}$ is the population decay rate. The intensity $x(t)$ is normalized to the saturation intensity $I_s = \gamma_{\perp}/2G$, with G the field–matter coupling constant. The population inversion $y(t)$ is normalized to the threshold inversion K_0/G; $z(t)$ is the modulation voltage normalized to $\pi/V_{\lambda/2}$, with $V_{\lambda/2}$ the $\lambda/2$ modulator voltage; A is the normalized pump parameter; β is the damping rate of the feedback loop; r is a coupling coefficient between the detected intensity $x(t)$ and the normalized $z(t)$ voltage; B is the bias voltage applied to the electro-optic modulator; and $\alpha = (1 - T)/T$.

The stationary solution (x^*, y^*, z^*) for the system [Eqs. (1)–(3)] implies the condition

$$B = rx^* + \arcsin(\{[A/(1 + x^*) - 1]/\alpha\}^{1/2}). \tag{4}$$

In Fig. 2 we show the stationary laser intensity versus one of the control parameters (B) for different values of the second parameter (r). This shows the coexistence of three fixed points for a wide range of r values. In Table 1 we present the numerical values for the eigenvalues and the corresponding normalized eigenvectors for the three stationary points consistent with Eq. (4) for $r = 0.16$, $A = 20/3$, and $\alpha = 9.0$ at $B = 0.838$.

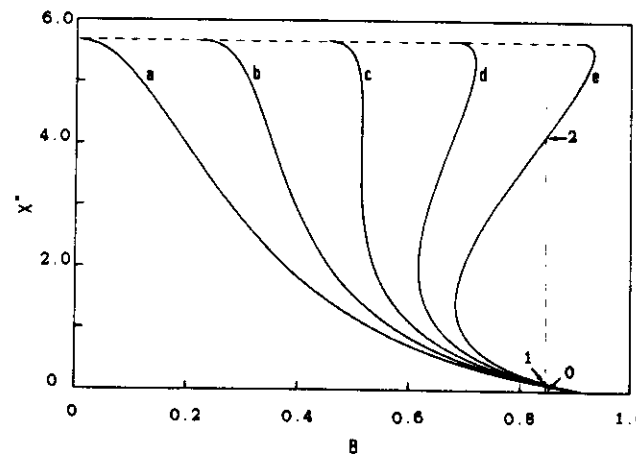

Fig. 2. Plot of the normalized stationary intensity x^* versus B for $A = 6.667$ and $\alpha = 9.0$. Curves a, b, c, d, and e refer to $r = 0.0$, 0.04, 0.08, 0.12, and 0.16, respectively. The horizontal dashed line corresponds to stationary solutions with $z^* = 0$. Points 0, 1, and 2, indicated by arrows, are the stationary points for $B = 0.838$ and $r = 0.16$.

Table 1. Eigenvalues and Eigenvector Components of the Fixed Points Shown in Fig. 2[a]

x^*	λ_i^R	λ_i^I	u_x^R	u_y^R	u_y^I	u_z^R	u_z^I
	+1.376	+0.000	+0.998	−0.058	0.000	−0.025	0.000
4.06	−1.013	0.133	0.986	+0.155	+0.033	0.052	+0.010
	−1.013	−0.133	0.986	+0.155	−0.033	+0.052	−0.010
	+0.109	0.536	0.788	−0.213	0.575	−0.028	0.041
0.16	+0.109	−0.536	0.788	−0.213	0.575	−0.028	−0.041
	−0.565	0.000	0.727	0.680	0.000	0.098	0.000
	+8.929	0.000	0.998	−0.057	0.000	−0.005	0.000
0.00	−0.077	0.000	0.000	1.001	0.000	0.000	0.000
	−0.258	0.000	0.000	0.000	0.000	1.001	0.000

[a] x^* indicates the stationary intensity values of Eq. (4) for $\alpha = 9.0$, $A = 20/3$, and $r = 0.16$ at $B = 0.838$. λ_i^R and λ_i^I, with $i = 0, 1, 2$, are the real and imaginary parts, respectively, of the eigenvalues at the ith stationary point. u_j^R and u_j^I, with $j = x, y, z$, are the normalized components of the eigenvectors calculated at the stationary point. All u_x^I are null for all eigenvalues.

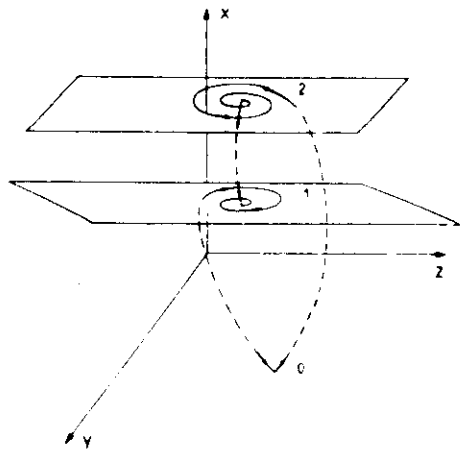

Fig. 3. Schematic view of a trajectory in the phase space when the dynamics are affected by all three unstable stationary points. The values of A and α are the same as in Fig. 2, with $r = 0.16$ and $B = 0.838$. The normalized components of eigenvectors are given in Table 1.

In Fig. 3 we present a schematic view of the trajectory in the three-dimensional space, obtained by a linear stability analysis of the motion around the stationary points, and qualitative connections between the linear manifolds (dashed lines).

EXPERIMENTAL RESULTS

From an experimental point of view we are able to visualize $(x - z)$ phase-space projections, obtained by feeding onto a scope the photodetector signal proportional to the laser output intensity $x(t)$ and the feedback voltage $z(t)$. This phase-space projection consists of closed orbits visiting successively the neighborhoods of the three unstable stationary points 0, 1, and 2.

The local chaos around point 1, established at the end of a subharmonic sequence, has been characterized by standard methods as power spectra and correlation dimension measurements.[9]

However, the existence of a global behavior characterized by pulses with regular shapes but chaotic in their time of

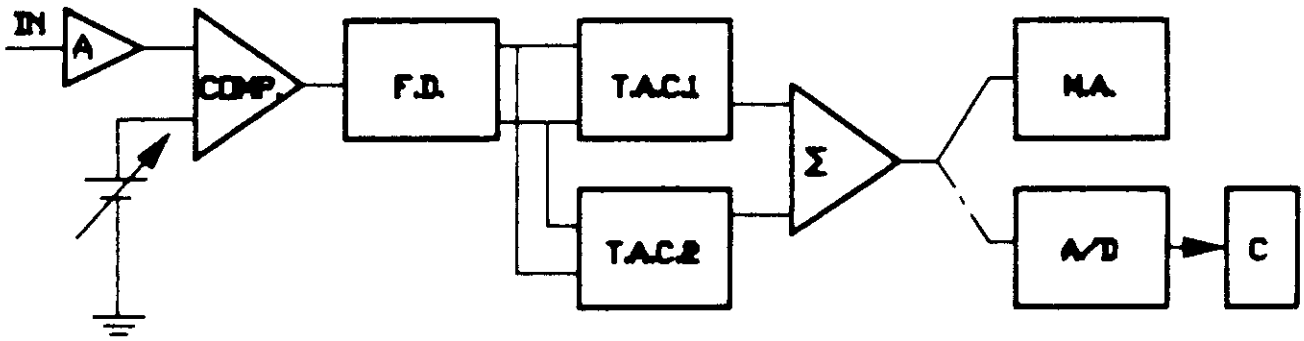

Fig. 4. Return-times measurement setup. COMP., comparator (threshold circuit); F.D., frequency divider; T.A.C.1, T.A.C.2, time-to-amplitude converters; M.A., multichannel analyzer; A/D, analog-to-digital converter; C, computer.

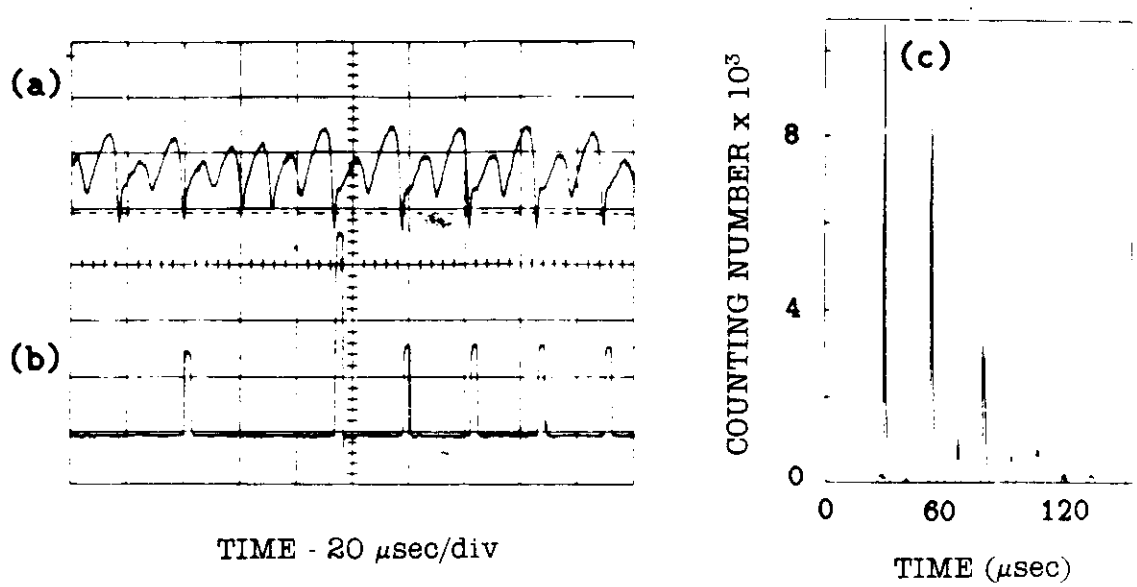

Fig. 5. (a) Time plot of the laser intensity at the onset of the Hopf bifurcation ($r = 0.330$ and $B = 0.270$). (b) T.A.C. pulses, whose heights are proportional to the return times to a Poincaré section $x(t)$ = constant [see the dashed line of Fig. 5(a)]. (c) Corresponding statistical distribution of return times.

occurrence makes it significant to study the dynamics through measurements of return times to a Poincaré section. The measurements have been done by using a threshold circuit like that shown in Fig. 4. An appropriate Poincaré section x = constant can be selected by adjusting the threshold level of our discriminator. The successive operation of time conversion has been done by means of two Canberra Model 2042 time analyzers. In our measurements we split into two separate channels the pulses corresponding to successive threshold crossings, and we use each of them as the start signal for one time analyzer and as the stop signal for the other.

One method to analyze the return times is based on the statistical distribution obtained by a multichannel analyzer. This method allows us to distinguish among the different dynamical regimes.

At the onset of the Hopf bifurcation the phase-space trajectory is a stable limit cycle around point 1, and the corresponding statistical distribution of return times [shown in Fig. 5(c)] shows a sharp peak. From the above distribution we evaluate an average return time τ_{av} = 9 μsec and a full width at half-maximum comparable with the accuracy of our measurement (i.e., 300 μsec/channel).

When B is increased at constant r, the limit cycle becomes unstable through successive subharmonic bifurcations and finally becomes chaotic. In this chaotic region we obtain a discrete distribution with peaks indicating the presence of high-order subharmonic bifurcations. The heights of the

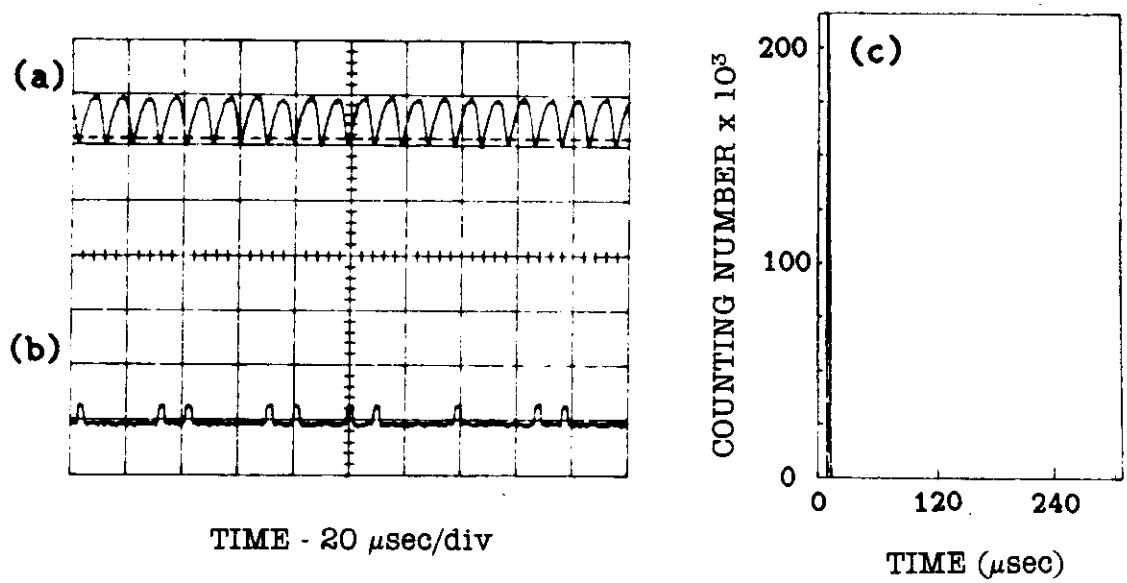

Fig. 6. (a) Time plot of the laser intensity. (b) T.A.C. pulses and (c) statistical distribution of return times for a local chaos around point 1 (r = 0.330 and B = 0.283).

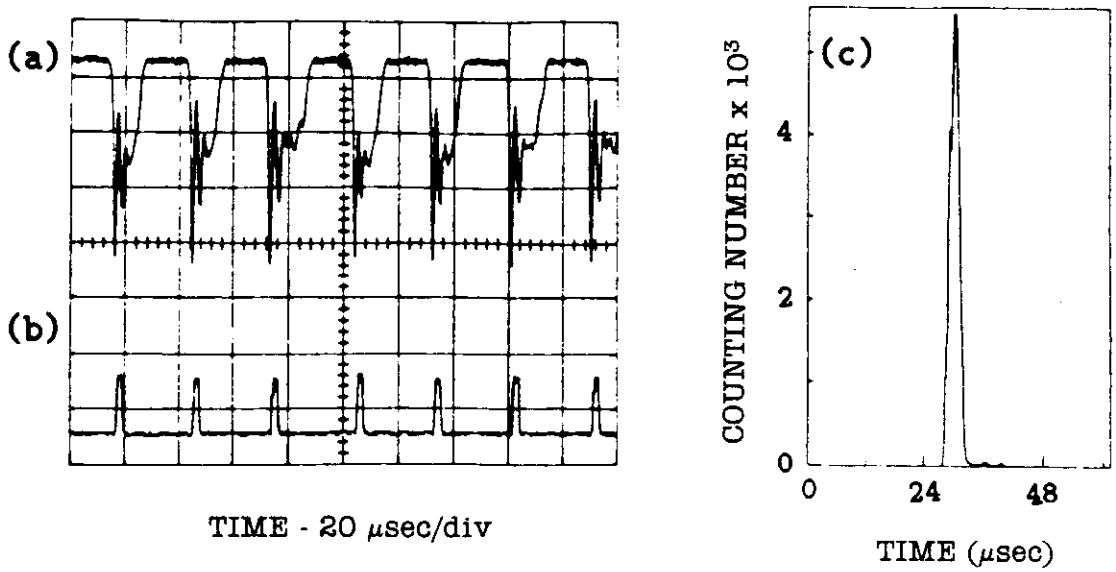

Fig. 7. (a) Time plot of the laser intensity. (b) T.A.C. pulses and (c) statistical distribution of return times in chaotic region of competing instabilities between points 1 and 2 (r = 0.380 and B = 0.285).

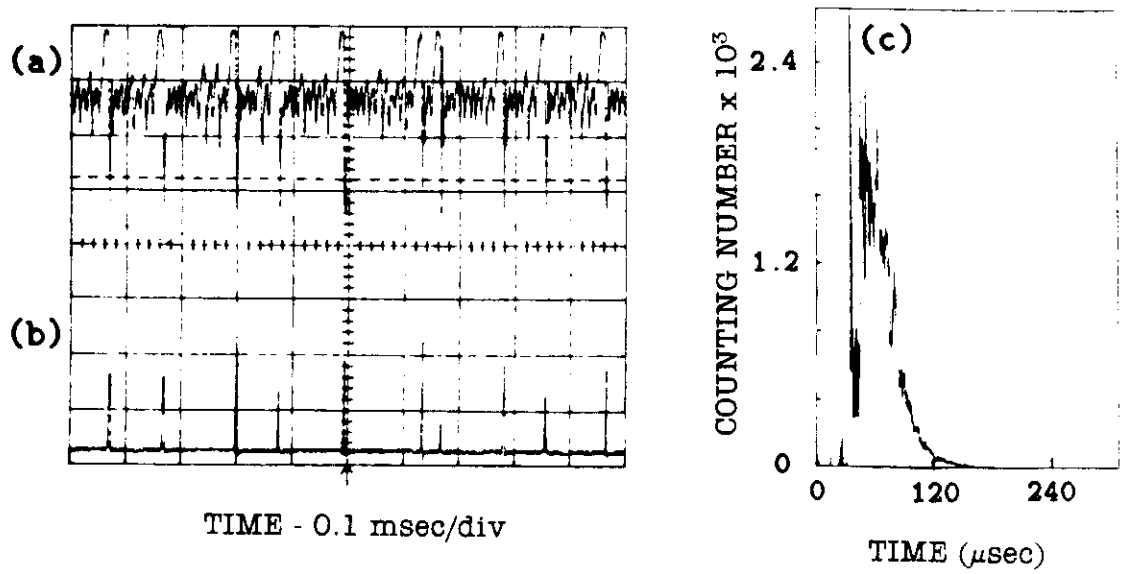

Fig. 8. (a) Time plot of the laser intensity. (b) T.A.C. pulses and (c) statistical distribution of return times in a window of Shil'nikov chaos (r = 0.430 and B = 0.340).

peaks in the distribution are strongly dependent on the setting of the threshold level [see Fig. 6(c)].

As B is increased further, we observe a progressive enlargement of the peaks up to a continuous distribution. In this case, the phase-space trajectory visits the neighborhoods of both points 1 and 2, which are competing for its determination. In Fig. 7 we refer to an experimental condition in which the competition is so strong that the corresponding statistical distribution becomes continuous with peaks superimposed [Fig. 7(c)].

Adjusting the control parameters in order to have a dominance of the saddle focus 2, we obtain a motion consisting of a quasi-homoclinic orbit asymptotic to it [Fig. 8(a)]. In this regime, the behavior of the laser output is characterized by pulses with regular shapes but chaotic in their recurrence. Based on such a consideration, the statistics of the return times appear to be the most appropriate characterization of this quasi-homoclinic chaos.

In Fig. 8(c) we show a statistical distribution corresponding to this regime. As we can observe, the statistical distribution is a broad featureless curve, which does not offer cues to the ordering of the return times τ_i. On the contrary, the iteration map (τ_{i+1} versus τ_i) displays an extremely regular structure that we show below to be in close agreement with that arising from Shil'nikov's theory of homoclinic chaos (see Fig. 9).

Before we discuss the details of Shil'nikov's theory, a crucial question arises: How much of the spread in the return times has to be attributed to point 2 or 0? Indeed, we have quasi-heteroclinic orbits visiting the surroundings of the two unstable points 2 and 0. But in our experimental situation the dynamics can be assimilated to a quasi-homoclinic orbit around point 2, which is thus mainly responsible for the spread in return times. This is easily proved by measuring the spread $\Delta\tau_0$ in the residence times τ_0 around 0 (zero intensity stripes) and the spread $\Delta\tau_2$ in the residence times τ_2 around 2 (complementary stripes, such that $\tau_0 + \tau_2$ is the total orbital time). In Fig. 10, which shows typical time sequences used to build the return map of Fig. 9, the two averaged relative spreads are approximately

$$\langle\Delta\tau_0\rangle/\langle\tau_0\rangle \sim 14\%, \qquad \langle\Delta\tau_2\rangle/\langle\tau_2\rangle \sim 80\%,$$

$$\langle\Delta\tau_0\rangle/\langle\tau_0\rangle \sim 40\%, \qquad \langle\Delta\tau_2\rangle/\langle\tau_2\rangle \sim 250\%.$$

The comparison shows that point 0 introduces a perturba-

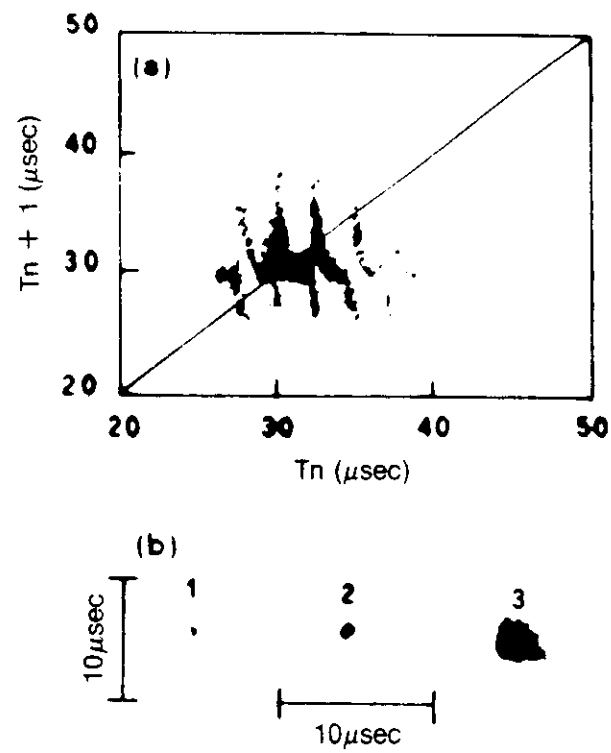

Fig. 9. Experimental iteration maps of the return times. (a) r = 0.487 and B = 0.350. (b) Maps corresponding to regular periodic situations, namely, 1, an electronic oscillator; 2, the laser in a regular periodic regime; 3, the laser just at the onset of the instability but still with a regular period.

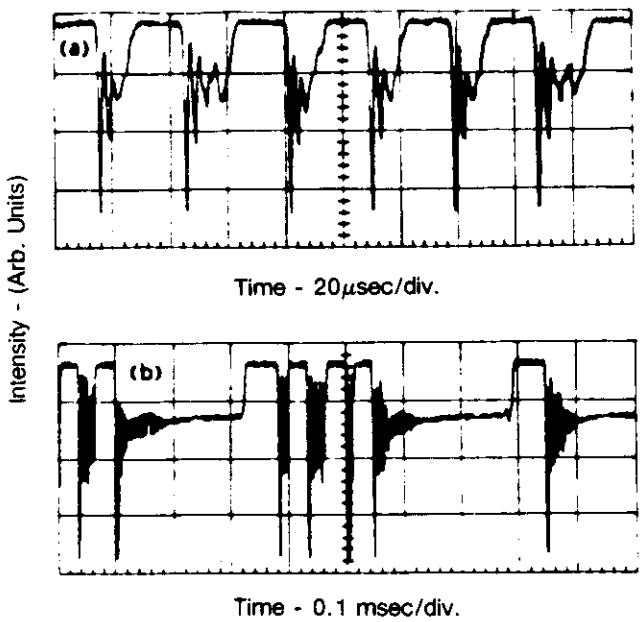

Fig. 10. Time plots of the intensity in the regime of Shil'nikov chaos. (a), (b) Refer to the same B value ($B = 0.427$) but two different gains r (0.487 and 0.696, respectively) of the feedback loop. (b) Shows long transients corresponding to a large number of small spirals around the saddle focus.

tion around 16% with respect to pure homoclinicity, that is, the orbital regularity is ruled mainly by point 2.

Thus a theoretical approach to our experiment in terms of homoclinic chaos appears justified.

UNIDIMENSIONAL ITERATION MAP

From a theoretical point of view, a homoclinic orbit asymptotic to a saddle focus can be modeled in terms of the following one-dimensional iteration map[15]:

$$\zeta_{n+1} = \zeta_n^{\lambda/\gamma} \cos[\omega/\gamma \ln(\zeta_n)] + \epsilon, \tag{5}$$

where γ and $-\lambda \pm i\omega$ are the eigenvalues of the linearized flow at the saddle focus, ζ is the coordinate along the unstable manifold, and ϵ is the deviation along ζ from the homoclinic orbit at the Poincaré section in the neighborhood of the saddle point ($\epsilon = 0$ corresponds to the homoclinic condition).

If we build a small cubic box of unit side centered at the saddle focus and oriented along the eigenvectors ξ, η, and ζ, and tiny difference in the entrance coordinate along the expanding axis ζ will strongly influence the residence time inside the box and hence the spacing from the next reinjection.

Observing that most of the time is spent in the box around the saddle point, we relate the return time τ to the coordinate ζ of the unstable manifold by $\zeta = \zeta_0 \exp(\gamma\tau)$, thus obtaining an iteration map for the return times[11]:

$$\begin{aligned} \tau_{n+1} &= -\ln[\exp(-\lambda/\gamma\tau_n)\cos(\omega/\gamma\tau_n) + \epsilon] \\ &= -\ln[\varphi(\tau) + \epsilon], \end{aligned} \tag{6}$$

where α, γ, ω, and ϵ are the same as above and we have collected in φ the terms that contain τ_n.

Comparison of Eqs. (5) and (6) shows the enhanced sensitivity to fluctuations of the τ map with respect to the ζ map. Indeed, suppose that the offset ϵ from homoclinicity is affected by a small amount of noise. The sensitivities of the two maps to such a noise are given, respectively, by $\partial\zeta/\partial\epsilon = 1$ and

$$\partial\tau/\partial\epsilon = [\varphi(\tau) + \epsilon]^{-1}. \tag{7}$$

This sensitivity factor acts as a lever arm whenever $\varphi(\tau) + \epsilon$ becomes very small. Note the following: (1) This is *not* deterministic chaos; in fact, large fluctuations can be expected even for a regular dynamics, implying a fixed point τ^* as shown in Fig. 9(b). (2) It is not associated with the homoclinicity condition $\epsilon = 0$; in fact, for finite ϵ there may a τ^* such that $\varphi(\tau^*) + \epsilon = 0$.

Since a homoclinic orbit is the dynamic counterpart of

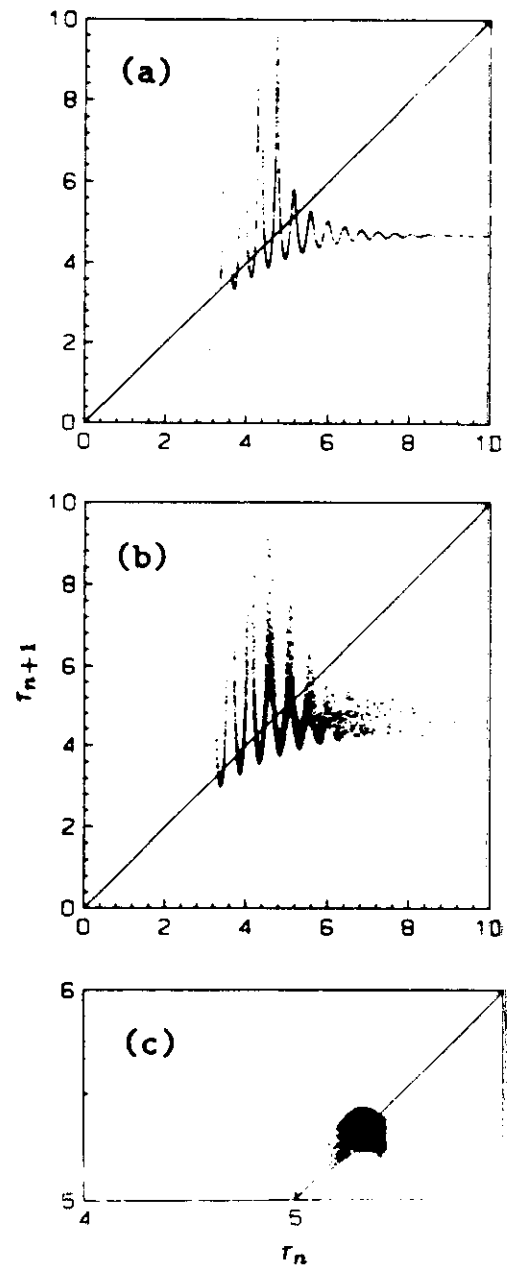

Fig. 11. Numerical iteration maps for Shil'nikov chaos. Parameter values: $\omega/\gamma = 13.0$, $\lambda/\gamma = 0.986$, $\epsilon = 0.01$. (a) and (b), τ maps without and with noise $\delta\epsilon = 10^{-2}$, respectively. (c) Stable fixed point of the regular dynamics, broadened by a noise $\delta\epsilon = 10^{-2}$.

repeated decays out of an unstable state, the result is like repositioning the initial condition in an experiment on a single decay. Here the repetition is automaticaly provided by the contracting motion asymptotic to the stable manifold. As a consequence, superposed upon the deterministic dynamics (either regular or chaotic), the high sensitivity [Eq. (7)] may provide a broadening of the τ maps not detectable in the ζ maps whenever noise in the offset ϵ is present.

In fact, the model description $\dot{x} = F(x)$ of a large system in terms of a low-dimensional dynamic variable x is just an ensemble-averaged description, and residual fluctuations on position x must be considered at some initial time, even though the successive evolution is accounted for by a deterministic law. In our case such a fluctuation is a stochastic spread $\delta\epsilon$ on the offset ϵ of the position ζ.

As shown in Fig. 11, the same amount of $\delta\epsilon$ in Eqs. (5) and (6) leaves the ζ maps unaltered, while it strongly affects the τ maps, making them appear like the experimental data.

If we specialize the map parameters α, γ, ω, and ϵ to a regular orbit (fixed points both in ζ and τ spaces), introduction of $\delta\epsilon$ does not broaden the ζ point, while the τ point broadens, in agreement with the experiment of Fig. 9(b). For example, the values $\alpha/\gamma = 0.98$, $\omega/\gamma = 2.98$, and $\epsilon = 0.01$ yield one fixed point $\tau^* = 5.327$, with a sensitivity $\partial\tau^*/\partial\epsilon = 182$ [Fig. 11(c)].

Note that the noise effect reported here has nothing to do with additive noise effects on return maps already described.[16] Indeed, the latter effects refer to the scaling behavior near stationary bifurcations, whereas our data refer to transient fluctuation enhancement, and they do not leave a permanent mark (such as an orbital shift or broadening).

Thus, while Shil'nikov chaos is a deterministic effect described on average by the backbone of the τ or ζ maps, the superposed thickening is a noise effect peculiar to τ maps and undetectable in ζ maps. This new effect is a specific indicator of intrinsic fluctuations, and it permits a demarcation line to be drawn between a real-life experiment and a model simulation, from which this second feature is absent.

CONCLUSION

We have shown a fundamental difference between a small system, ruled by a few equations, and a large system, in which the corresponding low-dimensional dynamics is a contracted description in terms of macroscopic variables, which are ensemble averages over some initial spread. In the latter case, the validity of a low-dimensional description depends on whether $\langle xx \rangle \simeq \langle x \rangle \langle x \rangle$, and this relation fails in decay situations such as Shil'nikov chaos, where we must couple the chaotic dynamic with statistical features.

In the small-system case the standard low-dimensional description of chaotic dynamics holds in terms of $\dot{x} = F(x)$ (x being a low-dimensional vector). In the large-system case the equation $\dot{x} = F(x)$ must be completed by an additional noise term; hence it becomes a high-dimensional (Langevin-type) equation $\dot{x} = [F(x), \xi(t)]$, where $\xi(t)$ is a stochastic process, not necessarily additive. In fact, we have shown that position noise is additive for ζ maps and multiplicative for τ maps.

ACKNOWLEDGMENTS

The authors thank S. Euzzor for help in the electronics. J. A. Roversi is the recipient of a fellowship from the National Research Council of Brazil. This research was partly supported by the European Economic Community.

F. T. Arecchi is also with the Department of Physics, University of Firenze, Firenze, Italy.

* Permanent address, University of Warsaw, Warsaw, Poland.

† Permanent address, Centro de Investigaciones en Laseres y Aplicaciones, Buenos Aires, Argentina.

‡ Permanent address, Universidade Estadual de Campinas, Campinas, S.P., Brasil.

REFERENCES

1. F. T. Arecchi, R. Meucci, and W. Gadomski, Phys. Rev. Lett. **58**, 2205 (1987).
2. L. P. Shil'nikov, Dokl. Akad. Nauk SSSR **160**, 558 (1965); L. P. Shil'nikov, Mat. Sb. **77**, 119, 461 (1968); **81**, 92, 123 (1970).
3. P. Glendinning and C. Sparrow, J. Stat. Phys. **35**, 645 (1984); P. Gaspard, R. Kapral, and G. Nicolis, J. Stat. Phys. **35**, 697 (1984).
4. F. Argoul, A. Arneodo, and P. Richetti, Phys. Lett. A **120**, 269 (1987).
5. F. T. Arecchi, A. Lapucci, R. Meucci, J. A. Roversi, and P. Coullet, submitted to Phys. Rev. Lett.
6. F. T. Arecchi, V. Degiorgio, and B. Querzola, Phys. Rev. Lett. **19**, 168 (1967).
7. F. Haake, Phys. Rev. Lett. **41**, 1685 (1978).
8. F. T. Arecchi and A. Politi, Phys. Rev. Lett. **45**, 1215 (1980); F. T. Arecchi, A. Politi, and L. Ulivi, Nuovo Cimento **71B**, 119 (1982).
9. F. T. Arecchi, W. Gadomski, and R. Meucci, Phys. Rev. A **34**, 1617 (1986).
10. F. T. Arecchi, in *Instabilities and Chaos in Quantum Optics*, F. T. Arecchi and R. G. Harrison, eds., Vol. 34 of Springer Series in Synergetics (Springer-Verlag, Berlin, 1987), p. 9.
11. F. T. Arecchi, R. Meucci, G. P. Puccioni, and J. R. Tredicce, Phys. Rev. Lett. **49**, 1217 (1982).
12. T. Midavaine, D. Dangoisse, and P. Glorieux, Phys. Rev. Lett. **55**, 1189 (1985).
13. F. T. Arecchi, G. L. Lippi, G. P. Puccioni, and J. R. Tredicce, Opt. Commun. **51**, 308 (1984).
14. G. L. Lippi, J. R. Tredicce, N. B. Abraham, and F. T. Arecchi, Opt. Commun. **53**, 129 (1985).
15. A. Arneodo, P. H. Coullet, E. A. Spiegel, and C. Tresser, Physica **14D**, 327 (1985).
16. J. P. Crutchfield, D. Farmer, and B. A. Hubermann, Phys. Rep. **92**, 45 (1982).